Letters

On the Surface Free Energy Anisotropy of UO₂

On the Surface Free Energy Anisotropy of UO_2

During a fundamental study of sintering phenomena in UO_2 [1], the high-temperature behaviour of isolated pores in UO_2 single crystals has been studied. Some observations on the shape of these pores will be reported here in connection with the anisotropy of surface free energy in crystalline solids.

The qualitative treatment of Herring [2] of the relation between the "γ-plot" (this is the radial plot of the surface free energy γ as a function of the direction) and the equilibrium shape of a small single crystal originally described by Wulff [3], stimulated systematic investigations of the surface free energy of different solids. The most widely used techniques are faceting of polished surfaces [4], the study of the equilibrium shape of very small crystals by coalescence of a thin evaporated layer [5], boundary grooving [6] and preferential dissolution [7]. These methods have been critically reviewed by Bikerman [8].

On the other hand, voids in solids have been intensively studied in connection with sintering processes and with irradiation behaviour of fissile and structural materials in nuclear technology. Under conditions of thermal equilibrium, pores can assume polyhedral shapes, bounded by planes and it has been shown that they behave like "negative crystals". Wolff and Hietanen [9] have described the analogous shape of "positive" and "negative" growth forms in connection with growth and dissolution phenomena.

The measurement of the equilibrium shape of pores in a solid requires special techniques in the field of metallography and microscopy but allows the study of pure surfaces, and thus avoids the problem of contamination which is of prime importance, as shown by Stranski [10] and Gjostein [11].

In quantitative studies, interactions between the pores and grain-boundaries must be avoided. This eliminates the conventional sintering techniques as a preparation method for the samples and calls for a method to generate pores inside a single crystal. Up to now, observations of voids and pores have been reported in molten or sintered UO_2 in which cases polyhedral shapes have sometimes been found.

Padden [12] describes isolated and grain-boundary located pores in sintered UO_2 of very high density, and observes pores bounded by both curved surfaces and planes, arranged with truncated octahedron symmetry. The planes we identified as the {100} and {111} planes, and the centres of the concentric growth steps were found to be along the [110] directions. Takahashi et al [13] investigated the microstructure of sintered UO_2 and observed a perfect cubic holohedral symmetry in pores located within the grains of hydrogen-sintered UO_2. The facets were indexed as {111}, {100} and {110}. In samples sintered in vacuo, pores were spherical with only small facets indexed as {111}, {100} and to a less extent {110}. These observations are consistent with the crystal habits observed by Robins et al [14]. Vapour-grown crystals show {111} and {100} habit, negative crystals {111}, {100} and {110}, while crystals prepared by molten salt electrolysis at lower temperature show {311} and {331} in addition. This is an expected result for an $Fm3M$ space group in which the forms {111}, {100}, {110}, {311}, {331} are of decreasing importance. The calculation of the anisotropy of surface free energy from the equilibrium shape is a direct consequence of the Wulff-theorem. The surface free energy of any body can be written in the form of an integral $\int \gamma(n)dS$, extended over the surface of the body, where the surface free energy is a function of the orientation of the unit outward normal n at each point of the surface.

This means that the equilibrium shape will tend to minimise the surface free energy by enlarging low free energy faces. It can easily be shown [16] that for two faces with surface free energy γ_1 and γ_2, the distance d_1 and d_2 between two parallel planes $h_1k_1l_1$ and $h_2k_2l_2$ will be:

$$\frac{d_1}{d_2} = \frac{\gamma_1}{\gamma_2}. \tag{1}$$

Considering a regular polyhedron consisting of eight {111} and six {100} faces, Nelson et al [17] expressed the total surface of this body in terms of two parameters, namely the distance (a) between opposite {100} faces and (b) the side of the square {100} faces, and minimised the expressions for constant volume. They obtained:

$$\frac{b}{a} \simeq \frac{1}{\sqrt{2}} \left(\sqrt{3} \frac{\gamma_{111}}{\gamma_{100}} - 1 \right). \qquad (2)$$

In the present investigation pores have been generated inside single crystals of UO_2 by thermal decomposition of U_2N_3 precipitates. UO_2 single crystals, grown from the vapour [15] were saturated with nitrogen by heating at 1900° C in a nitrogen atmosphere at atmospheric pressure. Subsequent slow cooling allowed precipitation of U_2N_3. Then the samples were quickly heated to 1900° C in argon containing oxygen at a partial pressure of 5 torr. This oxidation decreases the nitrogen solubility in UO_2 and avoids redissolution. Without cooling, the crystal is submitted to high vacuum for at least 10 h. This treatment generates spherical voids in the bulk of the crystal with diameters between 5 and 50 μm. The well-annealed and stoichio-
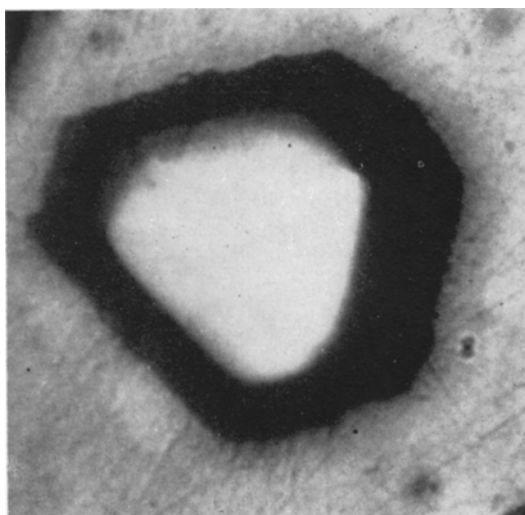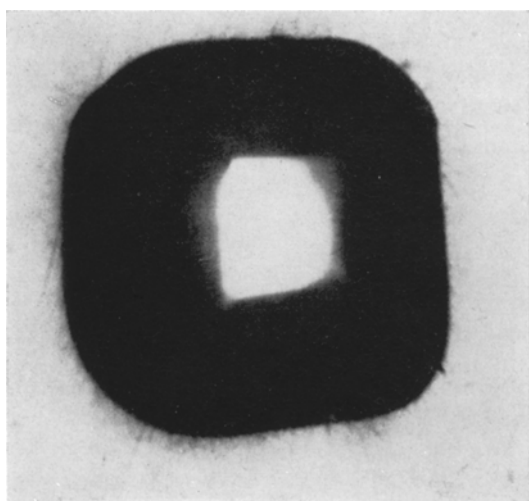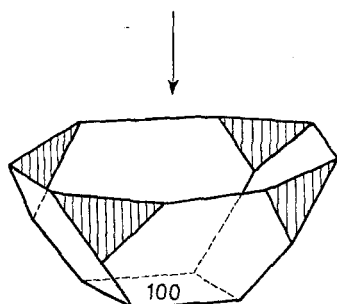

(a)
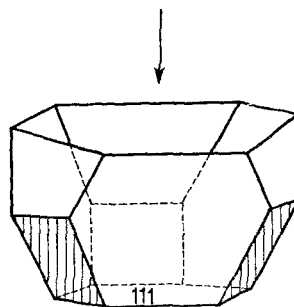
(b)

Figure 2 (a) Micrograph of pore cut by {111} plane and (b) theoretical shape ($\times$1500).

(a)

(b)

Figure 1 (a) Micrograph of pore cut by {100} plane and (b) theoretical shape ($\times$1500).

metric crystal contains not more than 300 ppm nitrogen.

Two different treatments have been applied to reach the equilibrium shape of the pores: for stoichiometric UO_2: 200 h at 1700° C under vacuum 10^{-5} torr; for hyperstoichiometric UO_{2+x}: 100 h at 1400° C at 5 torr oxygen. After 5 h of treatment *in vacuo*, the size and the shape of the pores remain constant. However, 200 h have been applied to be sure that equilibrium is attained and that strain generated in the lattice during the formation of the pores has been relieved. Fig. 1 and fig. 2 show typical micrographs of a pore, 30 μm in diameter, cut by a (1 1 1) and by a (1 0 0) plane. This form is the one for which Nelson *et al* [17] made their calculations. About 70 pores have been carefully measured and the value of a/b, as defined by Nelson *et al* [17], has been calculated. The

TABLE I

a/b	Number of observations f	Cumulative number of observations Σf	Procentual cumulative number of observations $\Sigma f \%$
2.90	1		
		1	1.4
2.90-2.95	3		
		4	5.5
2.95-300	7		
		11	15.3
3.00-3.05	12		
		23	32.0
3.05-3.10	20		
		43	59.7
3.10-3.15	18		
		61	84.8
3.15-3.20	6		
		67	93.0
3.20-3.25	4		
		71	98.7
3.25-3.30	1		
		72	100.0

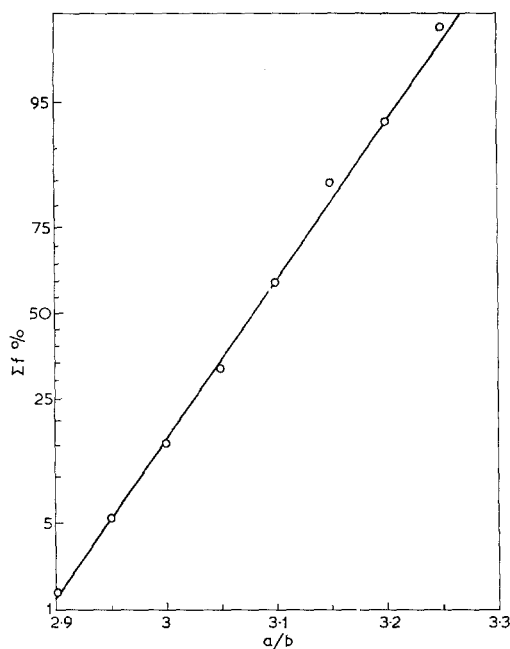$C = 3.08$; standard deviation (68%): 0.08.

Figure 3 Probability plot of measured a/b values.

statistical distribution of this value is shown in table I and has been plotted on probability paper in fig. 3. The idealised equilibrium form with the mean value $a/b = 3.08 \pm 0.08$ is shown on a Wulff net in fig. 4. Substitution of the value $a/b = 3.08$ in expression 2 gives:

$$\frac{\gamma_{100}}{\gamma_{111}} = 1.19 \pm 0.01 .$$

Mackenzie et al [18] calculated the anisotropy of free surface energy for face-centred and body-centred cubic crystals by considering geometrically the number of atoms per unit area which have exactly 1, 2, 3 . . . broken bonds. Taking $\gamma_{210} = 1$ they obtained:

$$\gamma_{110} = 0.949$$
$$\gamma_{100} = 0.895$$
$$\gamma_{111} = 0.775 .$$

The value $\gamma_{100}/\gamma_{111} = 1.19$ obtained in this study agrees fairly well with the value 1.152 calculated from the above results. Wells et al [20] performed calculations similar to the approach of Nelson and considered the ratio $\gamma_{111}/\gamma_{100}$ at which a {100} cube should transform into a {111} and {100} cubo-octahedron and further into a {111} octahedron. They obtained a value of 1.15 for the {111} {100} cubo-octrahedron to be the most stable form, which is in perfect agreement with both theoretical and experimental findings.

The oxidising treatment at 1400° C drastically changed the general aspect of the sample. The pores assumed a perfect spherical shape and all were located at grain-boundary intersections. The high mobility of the dislocations in hyper-stoichiometric UO_{2+x} which is responsible for

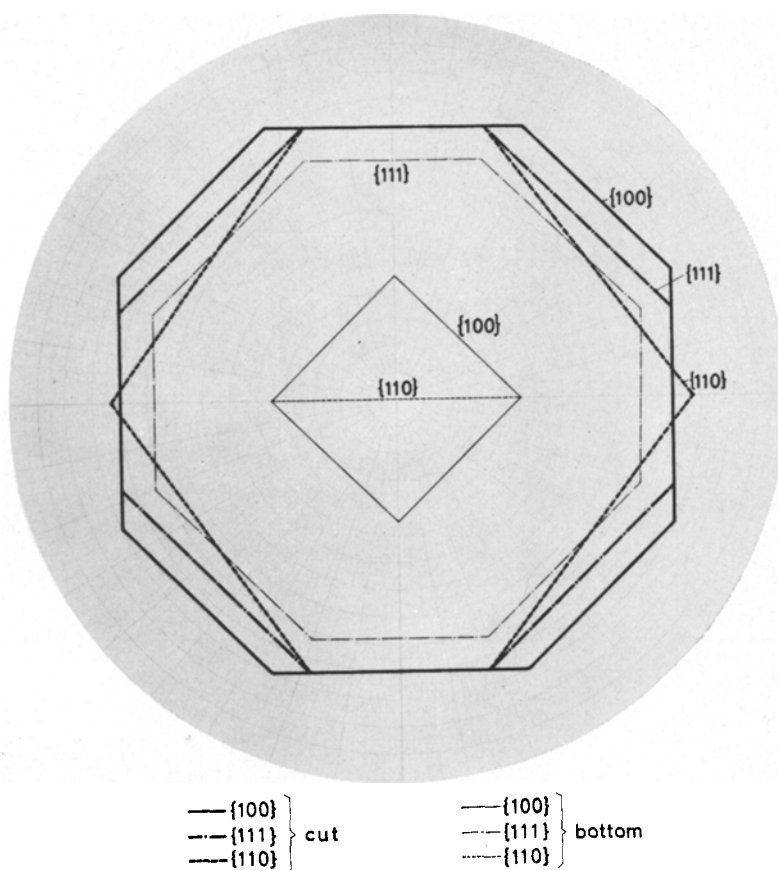|	
——{100} ⎤	——{100} ⎤
—·—{111} } cut	—·—{111} } bottom
—---{110} ⎦	········{110} ⎦

Figure 4 Wulff net projection of idealised pore shape, cut halfway.

the pronounced high-temperature plasticity of the material did result in the polygonisation of the sample, which became entirely polycrystalline (fig. 5). Although the oxygen dissociation pres-
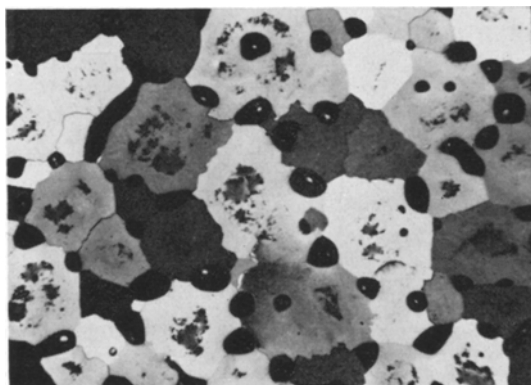

Figure 5 Micrograph of porous single crystals after oxidising treatment (×360).

sure of $UO_{2.20}$ at 1400° C (5 torr) and the rapid evaporation condensation processes can be responsible for the formation of partially rounded equilibrium shapes, we cannot offer, at the present time, a clear explanation of this isotropic behaviour. The most likely cause lies in the influence of the oxygen interstitials on the UO_2 lattice. It is clear that the introduction of interstitial oxygen atoms in the vicinity of the $(\frac{1}{2}, \frac{1}{2}, \frac{1}{2})$ position must strongly influence the free surface energy of the {110} planes, which are more affected than the {111} and {100} planes. In fact, the oxygen sub-lattice can be considered as a bcc lattice after introduction of a central oxygen interstitial, and in this structure the {110} and {111} faces have comparable free energies. Little is known about the mechanical properties of UO_{2+x} and U_4O_9 but it has been noticed that they have no preferential cleavage planes. Very recently Nadeau [19] showed that the increase in plasticity of UO_{2+x}

with increasing values of x is due to the removal of anisotropy in strength by nonstoichiometry. While the $\{100\}$ $<110>$ systems in stoichiometric UO_2 are much softer than the $\{1\bar{1}0\}$ $<110>$ systems, this anisotropy disappears in U_4O_9 or $UO_{2 \cdot 25}$.

References

1. W. VAN LIERDE, to be published.
2. C. HERRING, "Structure and Properties of Solid Surfaces", edited by Gomer Smith (1953).
3. G. WULFF, Z. Krist. 34 (1901) 449.
4. W. M. ROBERTSON, Acta Met. 12 (1964) 241.
5. B. E. SUNDQUIST, ibid 67.
6. W. M. ROBERTSON and P. G. SHEWMON, Trans. Met. Soc. AIME 224 (1962) 804.
7. M. B. IVES, J. Appl. Phys. 32 (1961) 1534.
8. J. J. BIKERMAN, Phys. Stat. Sol. 10 (1965) 3.
9. G. A. WOLFF and J. R. HIETANAN, Condensation and Evaporation of Solids, Proceedings of an Int. Symp., Dayton, 1962 (Gordon and Breach, 1964).
10. O. KNACKE and I. N. STRANSKI, Z. Elektrochem. 68 (1956) 816.
11. N. A. GJOSTEIN, Acta Met. 11 (1963) 956.
12. T. R. PADDEN and J. BELLE, Paris Conf. on Fuel, 1957.
13. S. TAKAHASHI, T. KUBOTA, H. DOI, and H. UCHIKOSHI, J. Atom. En. Soc. Japan 2 (1960) 7.
14. R. G. ROBINS, R. S. WILDS, and B. T. BRADBURY, J. Nucl. Mats. 5 (1962) 262.
15. W. VAN LIERDE, R. STRUMANE, E. SMETS, and S. AMELINCKX, ibid 5 (1962) 250.
16. P. G. SHEWMON and W. M. ROBERTSON, "Metal Surfaces" (Am. Soc. Metals, 1963) p. 67.
17. R. S. NELSON, D. J. MAZEY, and R. S. BARNES, UKAEA Report AERE-R-4564 (1964).
18. J. K. MACKENZIE and A. J. W. MOORE, J. Phys. Chem. Sol. 23 (1962) 185.
19. J. S. NADEAU, J. Amer. Ceram. Soc. 52 (1969) 1.
20. A. F. WELLS, Phil. Mag. 37 184 (1946) 605.

W. VAN LIERDE
Solid State Physics Dept
SCK-CEN
Mol, Belgium

Structure of Undercooled Hypoeutectic Cobalt-Tin Alloys

Earlier work on structure and properties of single-phase undercooled iron and nickel base alloys has shown a substantial modification of dendritic structure [1] and a considerable improvement of ductility [2] with increasing degree of undercooling prior to nucleation of the melt.

In the present study several ingots of hypoeutectic cobalt-10 wt % tin and cobalt-22.5 wt % tin alloys weighing approximately 100 g were solidified with various degrees of undercooling, table I. The experimental procedure used was that described previously [1, 2]. The cooling rate of the specimens after recalescence was 1° C sec^{-1}. Two ingots were surface-chilled [1] and cooled at 300° C sec^{-1}.

There is a substantial change in morphology of the primary cobalt-rich α-phase with increasing degree of undercooling, fig. 1, analogous to that observed in single-phase alloys [1, 2]. Thus, in the non-undercooled specimen the primary phase is equiaxed dendritic surrounded by a lamellar eutectic, fig. 1a. At moderate undercooling, e.g. 75° C, the primary phase exhibits a "cylindrical" dendritic morphology [1] and is also embedded in a lamellar eutectic matrix, fig. 1b. At high

undercooling exceeding 170° C the primary phase consists of uniform size spheres embedded in a discontinuous eutectic matrix, fig. 1c. Details of the spherical morphology are shown in fig. 2 which is a photomicrograph of a heavily etched specimen. The internal structure of the spheres is caused by solid state precipitation after completion of solidification during cooling of the ingot. These morphological changes with increasing undercooling are accompanied by a refinement of the dendrite arm spacing in the dendritic specimens and sphere diameter in the specimens of "spherical" morphology. A similar refinement is observed with increasing cooling rate. The explanation of these morphological variations is identical to that suggested for single-phase alloys [1].

Detailed measurements of the volume fraction of the primary phase revealed that it increases with increasing degree of undercooling. These measurements were made using a point counting technique [3]. Table I summarises the variation of weight fraction of the primary α-phase, f_α, versus degree of undercooling. Weight fractions were deduced from measured volume fractions assuming the specific weight of α to be $\rho_\alpha = 8.50$ g cm^{-3} and that of the cobalt-34 wt % eutectic $\rho_E = 8.40$ g cm^{-3}.

The variation of f_α with degree of undercooling